PCCP

PAPER

View Article Online
View Journal | View Issue

Cite this: *Phys. Chem. Chem. Phys.*, 2017, **19**, 7546

Ligand size dependence of U–N and U–O bond character in a series of uranyl hexaphyrin complexes: quantum chemical simulation and density based analysis†

Poppy Di Pietro*[a] and Andrew Kerridge*[b]

A series of uranyl complexes with hexaphyrin ligands are investigated at the density functional level of theory and analysed using a variety of density-based techniques. A relationship is identified between the size of the ligand and the stability of the complex, controlled by the presence of *meso*-carbon centres in the porphyrin ring. The complex with the smallest ligand, cyclo[6]pyrrole, is found to have enhanced covalent character in equatorial U–N bonds as defined by the quantum theory of atoms in molecules (QTAIM), as well as enhanced stability, compared to the larger complexes. QTAIM data are supported by electron density difference distributions, integrated electronic properties and analysis of the reduced density gradient (RDG), which all show unambiguous evidence of electron sharing in all U–N bonds. In all complexes, a weakening of the covalent axial U–O_{yl} interaction in comparison to free uranyl is found, with evidence for a separation of electronic charge resulting in a more ionic interaction. A relationship between covalent character in the U–N bonds and the magnitude of uranyl charge redistribution is identified, where the greater the covalent character of the U–N interaction, the more ionic the U–O_{yl} interaction appears. The complex with the largest ligand, hexaphyrin(1.1.1.1.1.1), is found to have additional interactions with the uranyl oxygen centres, perturbing the U–O_{yl} interaction.

Received 23rd December 2016,
Accepted 22nd February 2017

DOI: 10.1039/c6cp08783c

rsc.li/pccp

Introduction

Investigations of actinide coordination are challenging from both experimental and theoretical perspectives. Radioactivity and toxicity, amongst several other factors, hamper experimental study, while strong electron correlation, weak crystal fields and significant relativistic effects mean that the modelling of these complexes is not trivial.[1–6] However, developing our understanding of the bonding interactions of actinide elements is desirable from both a fundamental and practical perspective. The coordination chemistry of the actinides is a widely researched topic, with coordination by mono- and multi-dentate, as well as macrocyclic, ligands of great fundamental interest.[7–20] From a practical perspective, developing an improved characterisation of bonding in actinide complexes may be useful to, for example, the nuclear industry.

Worldwide, 10.9% of energy is now generated by nuclear fission,[21] with a typical reactor producing 20 metric tons of spent fuel per year.[22] This consists mainly of a mixture of uranium, plutonium, small amounts of the minor actinides neptunium, americium and curium, as well as fission products including lanthanides and transition metals. The amount of spent fuel generated is only likely to increase as the world becomes more reliant on fission power in order to meet growing energy demands, and how best to manage the long-lived and highly radiotoxic actinides in this spent fuel is an ongoing issue faced by the nuclear power industry. The minor actinides, whose chemistry is dominated by the trivalent oxidation state,[3] present a particular challenge as current practices for their management require efficient separation from the lanthanides, which exhibit very similar chemistry. For this reason, a significant research effort is currently focussed on the identification of ligands which show actinide selectivity.

To this purpose, relatively soft N-donor ligands have been investigated with varying degrees of success.[9] Several, such as ligands from the BTP, BTBP and BTPhen families, have exhibited promising selectivity,[23–25] however the source of this selectivity is not fully understood, and can be destroyed, or greatly enhanced, with small modifications to the ligand,[26–30] albeit not yet in a predictable way.

There is a growing body of work demonstrating that due to the actinide 5f-shell being relatively diffuse and extending beyond the

[a] *Department of Chemistry, University College London, 20 Gordon Street, London, WC1H 0AJ, UK. E-mail: poppy.pietro12@ucl.ac.uk*
[b] *Department of Chemistry, Lancaster University, Lancaster, LA1 4YB, UK. E-mail: a.kerridge@lancaster.ac.uk*

† Electronic supplementary information (ESI) available. See DOI: 10.1039/c6cp08783c

6d-shell, 5f orbitals have greater chemical availability.[6,11,31–34] Actinides are therefore potentially able to form bonds with a greater degree of covalency than lanthanides,[11,25,31,32,35–43] whose 4f orbitals are contracted and core-like.[9,37,39,43,44] The consequence of this is enhanced covalent character in the largely ionic An–N bonds, compared to similar Ln–N bonds, with this covalency conferring additional stability upon the actinide systems. This covalency is predicted to be most pronounced for the early actinides, decreasing across the series.[35–37,39,43]

The minor actinides Am(III) and Cm(III) behave very similarly to the lanthanides in terms of their bonding interactions,[3] hence the need for ligands which are highly selective. Covalency in complexes of the lanthanides and later actinides is weak,[39,45] thus any variations in covalent character is, commensurately, very small.[36–38,46–48] Uranium complexes have previously been considered as model systems[26,49–52] in studies of actinide covalency due to the aforementioned magnitude of covalent character in early actinides,[36,37,45–47,51] making any variation in covalency more apparent. Developing our understanding of the U–N interaction may therefore shed light on how covalency may be controlled and enhanced.

The expanded porphyrins are large, flexible, synthetic ligands capable of coordinating actinyl (di)cations in the equatorial plane[53–57] *via* pyrrolic nitrogen centres. The presence of *meso*-carbon centres between pyrrole units allows for modification to the size and shape of the ligand, and there are many possible substitution sites, allowing the possibility of ligands being 'tuned' to fit a specific cation.[57–60] Additionally, expanded porphyrins follow the CHON principle, a desirable criteria of an industrially useful separation ligand, specifically that it consist only of carbon, hydrogen, nitrogen and oxygen, which can be fully combusted after use to form environmentally safe products.

Several uranyl complexes with expanded porphyrin ligands have been experimentally realised. The hexaphyrins are expanded porphyrin macrocycles comprised of six pyrrolic subunits separated by varying numbers of *meso*-carbon atoms. Sessler *et al.* reported the synthesis of a uranyl complex of the hexaphyrin ligand isoamethyrin(1.0.1.0.0.0),[54] where the numbers in parentheses denote the number and position of *meso*-carbons (see Fig. 1), and suggested its possible use as a colorimetric actinide sensor.[54,61] The Sessler group has also reported neptunyl and plutonyl complexes with isoamethyrin[54,62] as well as several other expanded porphyrins and similar expanded porphyrin-like macrocycles,[55] and uranyl complexes of the hexaphyrin ligands cyclo[6]pyrrole (comprising no *meso*-carbons) and amethyrin(1.0.0.1.0.0).[53,56] Uranyl complexes of the rubyrin(1.1.0.1.1.0), rubyrin(1.1.1.1.0.0) and hexaphyrin(1.1.1.1.1.1) ligands have not been reported, however the ligands themselves have been synthesized either as free-base macrocycles or complexes of, for example, transition metals.[57,60,63–74] To date, many different expanded porphyrin ligands have been synthesised.[57,58,71,75–80] Due to the existence of many possible substitution sites, the basic hexapyrrolic structure of the ligands may be modified with peripheral or *meso*-substituents,[63,71,72,81–83] or for example, replacement of a pyrrolic subunit with a different kind of ring, *e.g.* a furan or pyridine subunit.[84] Actinide and actinyl complexes of several other expanded porphyrin-type ligands have been reported and investigated both experimentally and theoretically.[85–93]

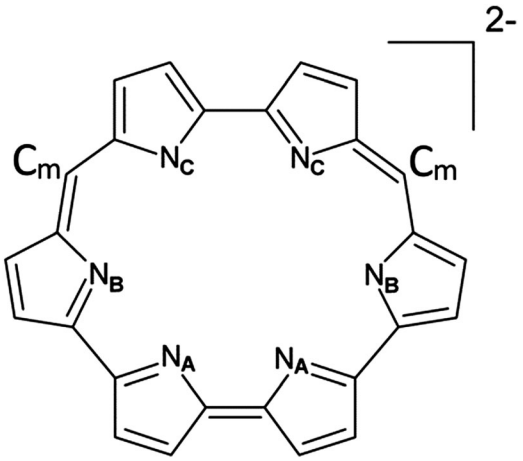

Fig. 1 Molecular structure of isoamethyrin dianion omitting peripheral groups for clarity. Symmetry-distinct coordinating nitrogens are labelled N_A, N_B and N_C. *meso*-Carbon atoms are labelled C_m.

Although the equatorial bonding characteristics of uranyl, with its formally empty 5f-shell, and the trivalent minor actinides with their partially filled f-shells are expected to differ, it is intended in this instance simply to investigate the potential for expanded porphyrin ligands to coordinate a uranyl dication and to quantify the nature of the U–N bonds in such complexes with the aim being to begin to identify the characteristics of a ligand which lead to increased equatorial covalency. In this way, if the selectivity shown by ligands from the BTP/BTBP/BTPhen families is indeed covalency driven, results obtained here may be useful for informing the design of future selective ligands. Additionally, the presence of the distinctive and experimentally accessible U–O_{yl} stretching modes[94–96] may act as probes of equatorial covalency.[97] Ultimately it is intended that this work will be extended to include complexes of uranyl and plutonyl, and perhaps eventually the trivalent minor actinides.

Previously, we have performed an in-depth study on the equatorial coordination behaviour of uranyl with a range of monodentate first row ligands.[97] Using density based analysis, we determined a strong correlation between covalent character in equatorial bonding and the vibrational frequencies of the U–O_{yl} stretching modes. Subsequently, we compared two complexes of uranyl with multidentate ligands:[98] a complex with the hexadentate macrocyclic expanded porphyrin ligand isoamethyrin and a complex with two tridentate bis-triazinylpyridine (BTP) ligands which have been shown to act selectively for An(III) over Ln(III) in industrial separation processes. Our theoretical study concluded that the U–N bonding in these two complexes was strongly similar: largely ionic equatorial bonds with a comparable degree of covalency and a commensurate weakening of the U–O covalent interaction suggesting a redistribution of charge in the uranyl unit, with the very similar equatorial bonding in the two complexes suggesting that expanded porphyrin ligands may be interesting candidates for future investigations of actinide selectivity.[98]

In this contribution, we combine quantum chemical calculations at the density functional (DFT) level of theory with density-based analysis techniques to show that complexes of uranyl with hexaphyrin ligands provide an interesting set of systems for investigating covalency in the U–N interaction. We determine the effect of altering the size of the ligand core on the degree of covalent character in equatorial U–N bonds, and quantify the extent of the charge redistribution in the uranyl unit that occurs upon complexation using the experimentally accessible U–O_{yl} stretching frequencies.

Quantum chemical calculations have been used to investigate eight complexes in total, of which three have previously been synthetically realised: UO_2-cyclo[6]pyrrole, which contains no *meso*-carbon atoms, as well as UO_2-isoamethyrin(1.0.1.0.0.0) and UO_2-amethyrin(1.0.0.1.0.0) which each contain two *meso*-carbon atoms. Additionally, four hypothetical complexes with synthetically realised ligands are studied: UO_2-rubyrin(1.1.1.1.0.0), UO_2-rubyrin(1.1.1.0.1.0), UO_2-rubyrin(1.1.0.1.1.0), which each contain four *meso*-carbon atoms, and UO_2-hexaphyrin(1.1.1.1.1.1) which contains six, one bridging each of its pyrrolic subunits. Finally, one system for which both the complex and the ligand are hypothetical, UO_2-hexaphyrin(1.1.0.0.0.0), has been investigated. These ligands were selected so that the effect of increasing the size of the hexaphyrin core *via meso*-substitution could be directly investigated.

All complexes have been optimised at the density functional level of theory and, as a representative sample, four complexes were selected for detailed density analysis. For simplicity, the eight complexes will be referred to throughout using the labelling defined in Table 1.

In order to avoid any potential ambiguities that may arise from employing orbital-based analysis techniques, we focus on electron-density based analytical approaches. Such density-based analyses have previously been successfully applied to f-element complexes[14,36–39,42,47,99,100] and, in particular, allow direct comparison of results obtained using DFT with those obtained using multiconfigurational methodologies.

The quantum theory of atoms in molecules[101,102] (QTAIM) has been used to assess covalent character in U–N and U–O bonds. QTAIM relies upon the partitioning of a molecule into atomic basins bound by surfaces satisfied by the condition $\nabla\rho(\mathbf{r})\cdot\mathbf{n}(\mathbf{r}) = 0$. $\mathbf{n}(\mathbf{r})$ is the unit vector normal to the basin surface. Points at which the gradient in the electron density vanishes, $\nabla\rho(\mathbf{r}) = 0$, define the critical points in $\rho(\mathbf{r})$. Of particular interest in this study are "bond critical points" (BCPs), which are found where the line of maximum density defining a bond path between bonded atoms is at its minimum.[103] Values of topological indicators at the BCP characterise the bonding interaction. In general, where the BCP has $\rho > 0.20$ a.u. and $\nabla^2\rho < 0$, a bond can be described as covalent. Broadly speaking, the higher the value of ρ, the higher the covalent character of the bond. The energy density, H, can also be used as a measure of covalency.[101,102] For a covalent bond, its value is expected to be negative, with the degree of covalency indicated by the magnitude. In addition, integrated properties such as atomic populations, as well as localisation and delocalisation indices can be obtained by integrating over atomic basins and give insight into both electron sharing and charge donation.

We complement our QTAIM studies by considering regions of weak interaction,[104] by investigating the reduced density gradient (RDG), defined as $s(\mathbf{r}) = |\nabla\rho(\mathbf{r})|/2(3\pi^2)^{1/3}\rho(\mathbf{r})^{4/3}$, and, finally, visualise electron density difference distributions upon complexation to qualitatively analyse the changes that are undergone upon complex formation. We compare these distributions to our quantitative data in order to develop a comprehensive description of the nature of U–N and U–O bonding in these complexes.

Table 1 Complex naming convention used in this study. The subscript refers to the number of *meso*-carbon atoms

	Simplified complex	Substituted complex
Cyclo[6]pyrrole	C_0	C_0'
Hexaphyrin(1.1.0.0.0.0)	C_2a	C_2a'
Isoamethyrin(1.0.1.0.0.0)	C_2b	C_2b'
Amethyrin(1.0.0.1.0.0)	C_2c	C_2c'
Rubyrin(1.1.1.1.0.0)	C_4a	C_4a'
Rubyrin(1.1.1.0.1.0)	C_4b	C_4b'
Rubyrin(1.1.0.1.1.0)	C_4c	C_4c'
Hexaphyrin(1.1.1.1.1.1)	C_6	C_6'

Computational details

Density functional theory (DFT) calculations have been performed using version 6.4 of the TURBOMOLE quantum chemistry software package.[105] Ahlrichs def2-TZVP basis sets of triple-zeta quality have been used for the C, H, O and N atoms[106] and the Ahlrichs def-TZVP basis set of triple-zeta quality, which incorporate a relativistic ECP comprising 60 core electrons[107] has been used for the U atoms. All complexes summarised in Fig. 2 and 3 were optimised using the PBE exchange–correlation xc-functional[108] which employs the generalised gradient approximation (GGA). Subsequent reoptimisation of a representative sample of complexes was also performed using the B3LYP

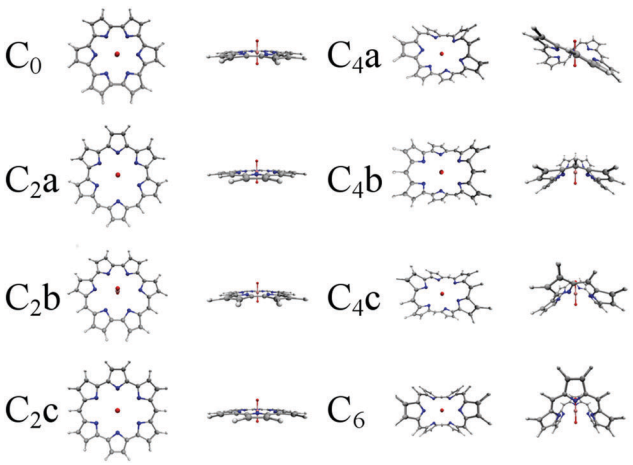

Fig. 2 Optimised structures of the eight uranyl hexaphyrins considered in this study, optimised in the gas phase using the PBE exchange–correlation functional, without peripheral alkyl substituents.

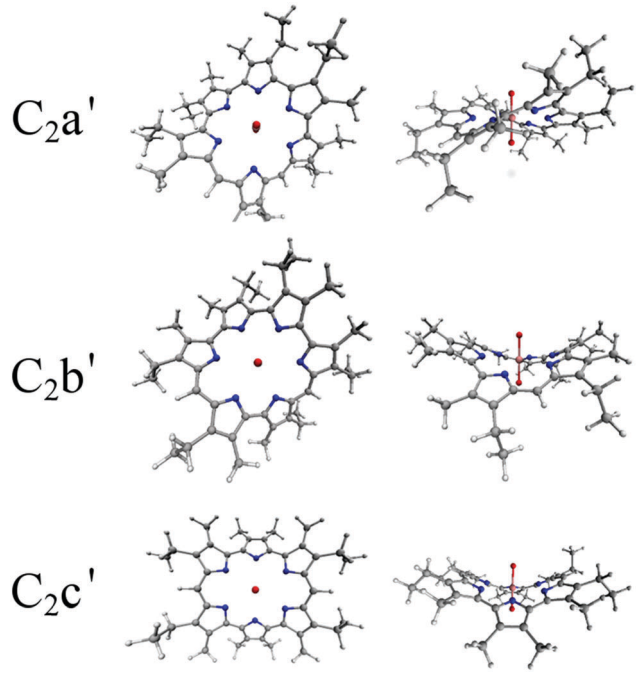

Fig. 3 Optimised peripherally substituted C_2 structures, optimised in the gas phase using the PBE exchange–correlation functional.

hybrid-GGA xc-functional[109,110] to approximate the exchange correlation energy. This was done in order to investigate the effects of incorporating exact exchange on properties of the electron density. Both PBE and B3LYP have previously be shown to be suitable for the accurate modelling of actinide-containing systems.[3,14,97,98,111,112] Initial optimisations were carried out in the gas phase. Subsequently, the COSMO continuum solvation model,[113] using a relative permittivity of ε_r = 8.9 was used to simulate solvation in DCM, for which there is experimental precedent.[54] Vibrational analysis was performed to ensure that structures represented energetic minima.‡ Due to the closed shell nature of these systems, the effects of spin–orbit coupling were not included in the calculations.

All of the hexaphyrin macrocycles reported experimentally feature methyl substituents on the periphery of their pyrrole units (see Fig. 3). These are generally assumed to have little effect on the geometry and electronic structure of the molecule and in order to minimise computational expense, such substituents are often omitted when performing DFT simulations. However it has been shown that for UO_2-isoamethyrin(1.0.1.0.0.0), this simplification leads to severely overestimated (by ~0.1 Å) U–N bond lengths.[114] Thus, as with our previous study comparing UO_2-isoamethyrin(1.0.1.0.0.0) with $[UO_2(BTP)_2]^{2+}$, optimisations have been performed with and without these substituents so that their effects on geometry could be assessed. U–N and U–O bond lengths have been compared to experimental data where available. For electron density analysis, single point energy calculations were performed at the optimised geometries using the SARC all-electron uranium basis set[115] and the second-order Douglas–Kroll–Hess (DKH2) Hamiltonian to account for scalar relativistic effects.[116,117] QTAIM analysis was performed using the Multiwfn[118] and AIMAll[119] codes in order to calculate topological and integrated properties of the electron density. RDG and density difference data were visualised using the VMD code.[120]

‡ Due to computational expense, vibrational frequency analysis was not performed on the C_2b' complex when optimised with the B3LYP functional. Similarly, large peripherally substituted complexes, with the exception of C_2b' which was selected for further study, were optimised using only the PBE functional.

Results and discussion

Geometrical characterisation and energetic stability

Geometries of the complexes optimised using the PBE xc-functional in the gas phase are shown in Fig. 2 and 3. It is apparent (see Table S1, ESI†) that, in most cases, the inclusion of peripheral alkyl groups has a relatively small effect on the average U–N bond length, with differences of only a few hundredths of an Angstrom, and results in no significant structural variation. The exception is with the C_2x complexes, in which simplified and substituted forms have differences in average bond lengths of approximately 0.1 Å, nearly an order of magnitude higher than for the C_0, C_4 and C_6 complexes. All C_2x complexes exhibit significant structural variation when peripheral substituents are included, with a degree of non-planarity introduced that acts to shorten the U–N bonds. Based on these results, C_0, C_4x and C_6 complexes will all be considered in their simplified form for the remainder of this contribution, and substituents will only be considered in the case of the C_2x complexes, with the substituted system referred to as C_2x'. Table 2 summarises U–N bond lengths for the complexes C_0, C_2x', C_4x and C_6 and U–O bond lengths can be found in Table 3.

An examination of U–N and U–O bond lengths reveals that complex C_0 has the shortest average U–N bond lengths of all eight complexes, 2.532 Å (2.527 Å), when optimised in the gas phase (DCM). C_0 features four longer and two slightly shorter (by ~0.01 Å) U–N bonds. This complex also has the longest calculated U–O bond length, 1.799 Å (1.812 Å), when optimised in the gas phase (DCM), thereby exhibiting the strongest perturbation of the uranyl unit due to equatorial complexation. Additionally, a very slight degree of non-planarity is introduced upon solvation (and upon addition of peripheral substituents), although this causes no significant changes to bond lengths. When compared to experimental values, the U–N bond lengths of C_0 are reproduced to within 0.01 Å (0.01 Å) in the gas phase (DCM), an excellent level of agreement, while the U–O bonds

Table 2 Ranges of U–N bond lengths in Å for complexes optimised using the PBE exchange–correlation functional in the gas phase/*DCM*

Complex	r_{U-N} (gas phase/*DCM*)	$\overline{r_{U-N}}$
C_0	2.528–2.534/*2.522–2.530*	2.532/*2.527*
C_2a'	2.591–2.835/*2.591–2.812*	2.673/*2.659*
C_2b'	2.586–2.772/*2.573–2.755*	2.688/*2.674*
C_2c'	2.569–2.751/*2.557–2.736*	2.689/*2.674*
C_4a	2.533–2.827/*2.527–2.811*	2.717/*2.706*
C_4b	2.690–2.720/*2.678–2.700*	2.701/*2.687*
C_4c	2.663–2.785/*2.654–2.769*	2.703/*2.692*
C_6	2.640–2.820/*2.637–2.818*	2.700/*2.697*

Table 3 U–O bond lengths in Å for complexes optimised using the PBE exchange–correlation functional in the gas phase/*DCM*

Complex	r_{U-O} (gas phase/*DCM*)
C_0	1.799/*1.812*
C_2a'	1.789/*1.802*
C_2b'	1.787/*1.799*
C_2c'	1.787/*1.800*
C_4a	1.784/*1.793*
C_4b	1.783/*1.792*, 1.785/*1.793*
C_4c	1.784/*1.792*
C_6	1.784/*1.791*, 1.789/*1.796*
UO_2^{2+}	1.711/*1.721*

are reproduced to within 0.02 Å (0.03 Å) in the gas phase (DCM), a good level of agreement.[53] It is worth mentioning that the crystal structure of C_0 exhibits nearly perfect planarity, in agreement with the calculated gas phase structure.

Moving on to the complexes containing two *meso*-carbons, the simplified complexes C_2a, C_2b and C_2c share several characteristics. All are perfectly or very nearly planar, with average U–N bond lengths of 2.776–2.804 Å (2.770–2.799 Å) when optimised in the gas phase (DCM) and U–O bonds of 1.777–1.778 Å (1.786–1.793 Å) when optimised in the gas phase (DCM). Our calculated U–N and U–O bond lengths for both C_2b and C_2b' are in good agreement with the previous theoretical values reported by Shamov and Schreckenbach,[114] and, for C_2b', structural parameters are in good agreement with experimental data.[54] Shamov and Schreckenbach's work illustrated the importance of including these substituents when modelling uranyl isoamethyrin, and here we find that substituents have a similar distorting effect on both C_2a' and the hypothetical C_2c', where a presumably sterically-induced twisting of the ligand results in average U–N bond lengths of 2.673–2.689 Å (2.659–2.674 Å) when optimised in the gas phase (DCM), ~0.1 Å shorter than their simplified analogs. Commensurately, U–O bonds in the C_2x' complexes are slightly longer than their simplified analogs, 1.787–1.789 Å (1.799–1.802 Å) when optimised in the gas phase (DCM). These differences demonstrate that careful consideration of the effects of substituents and solvation models is essential when modelling hexaphyrin complexes. It may be interesting to investigate the rigidity of these structures using perhaps MD simulations, although this has not been performed as part of this study.

Non-planarity in C_4a, C_4b and C_4c is pronounced. Average U–N bond lengths are typically a few hundredths of an Angstrom longer than for the C_2x' complexes, 2.701–2.707 Å (2.692–2.706 Å) when optimised in the gas phase (DCM). U–O bonds are commensurately slightly shorter than those in the C_2x' complexes, 1.783–1.785 Å (1.792–1.793 Å) when optimised in the gas phase (DCM).

C_6, the largest complex, is also highly non-planar, allowing equatorial U–N bonds of comparable length to the C_2x' and C_4x complexes to be formed. Interestingly, in this complex the ligand is folded almost completely in half (reminiscent of a Pacman-style ligand[16,89,121,122]), although here the uranyl unit is coordinated at the ligands centre. This folding has the effect of bringing some ligand atoms significantly closer to the –yl oxygen ions than in any of the other complexes. Average U–N bonds are 2.700 Å (2.697 Å) when optimised in the gas phase (DCM). U–O bond lengths are 1.789 Å (1.796 Å) and 1.784 Å (1.791 Å), with an 0.005 Å elongation of one bond due to the aforementioned C–O_{yl} interaction.

Reoptimisations of C_0, C_2b', C_4a, and C_6 were performed using the hybrid B3LYP functional but led to no significant structural changes. U–N bond lengths were calculated to be in the region of 0.005 Å longer and U–O bond lengths were found to be shorter by approximately the same amount. Irrespective of the functional employed, continuum solvation acts to give a slight shortening of the U–N bonds and a corresponding lengthening of U–O bonds.

Binding energies

Complex stability was investigated by calculating molecular binding energies as well as ligand deformation energies. Molecular binding energies (ΔE) were calculated as defined in eqn (1) by subtracting the energies of the optimised uranyl dication and ligand dianion fragments from that of the complex:

$$\Delta E = E_C - (E_{UO_2^{2+}} + E_{L^{2-}}) \quad (1)$$

The highly flexible nature of the macrocyclic ligands considered here is such that it is informative to evaluate the degree by which the fragments deform from their optimal geometries upon complexation. Ligand deformation energies (E_{DL}) were calculated by subtracting the energy of each ligand in its coordination geometry from that of the optimised free ligand, as in eqn (2):

$$E_{DL} = E_{L^{2-}}^{Opt} - E_{L^{2-}}^{Coord} \quad (2)$$

And similarly for the uranyl dication:

$$E_{DU} = E_{UO_2^{2+}}^{Opt} - E_{UO_2^{2+}}^{Coord} \quad (3)$$

The deformation energies may be considered independently or subtracted from the calculated binding energy to obtain a deformation adjusted binding energy (E_{DA}).

$$\Delta E_{DA} = \Delta E - (E_{DL} + E_{DU}) \quad (4)$$

In this way, complex stabilities can be considered in a manner that allows for the effects of the destabilisation of the uranyl and hexaphyrin fragments to be taken into account.

Molecular binding energies and deformation adjusted binding energies calculated from PBE gas phase optimisations are listed in Table 4. The overall trend is for binding energies to fall as the ligands become larger, decreasing by ~1.5 eV from C_0 to the C_2x' complexes, then by another ~1.5 eV from the C_2x' to the C_4x complexes, where the effect appears to plateau. There is a decrease of only ~0.2 eV from the C_4x complexes to the C_6 complex. Notably, the complexes predicted to be most stable here, C_0 and C_2x', are those that have been synthetically realised, while the less stable C_4x and C_6 complexes have proven, so far, to be experimentally inaccessible.

It is interesting to note that the deformation energy of the ligand increases as the core size is increased. This increase is ~1 eV per pair of *meso*-carbon up to the C_4x complexes,

Table 4 Molecular binding energies in (ΔE) and deformation adjusted binding energies (ΔE_{DA}), with deformation energies of the UO_2^{2+} unit (E_{DL}) and the ligands (E_{DU}), all given in eV. Data was obtained using the PBE xc-functional, and due to the simple COSMO solvation model being a rather poor approximation for solvated uncoordinated UO_2^{2+}, are given in the gas phase only

	ΔE	ΔE_{DA}	E_{DL}	E_{DU}
C_0	−29.40	−30.37	0.25	0.38
C2a′	−28.17	−29.52	1.05	0.30
C2b′	−27.96	−29.26	1.02	0.29
C2c′	−28.05	−29.30	0.96	0.29
C4a	−26.26	−28.51	1.98	0.27
C4b	−26.03	−28.39	2.09	0.27
C4c	−26.17	−28.46	2.03	0.27
C6	−26.07	−28.16	1.80	0.28

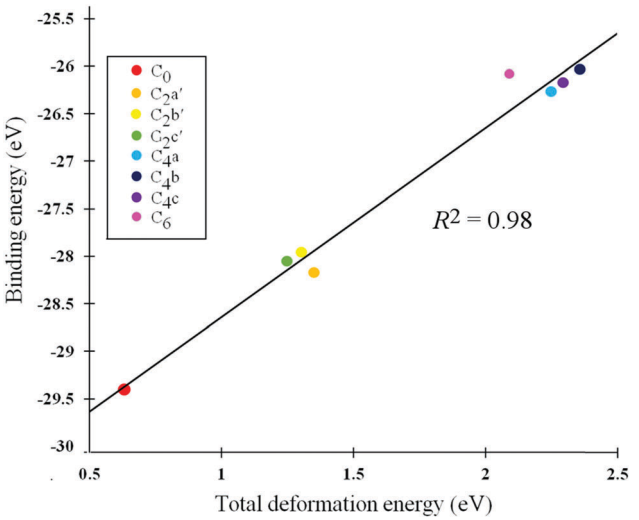

Fig. 4 Molecular binding energy plotted against total deformation energy for all eight complexes. Energies are taken from the structures optimised in the gas phase.

which appear to represent a maximum. Beyond this, increased flexibility in the ligand presumably reduces the deformation energy penalty. The deformation energy of the uranyl unit decreases slightly as the ligand core size increases: it is comparable, and in fact dominant, to that of the ligand in C_0, whereas it is of comparable magnitude in all other complexes studied. Combined, the result is a net increase in deformation energy from C_0 to C_6. Whilst the deformation energy doesn't fully account for the relative stability of the smaller ligands, it does strongly correlate (R^2 = 0.98) as shown in Fig. 4.

When the deformation energy is subtracted from the binding energy to obtain a deformation adjusted binding energy, the relationship between binding energy and ligand size persists and there is a loss of stability for each pair of *meso*-carbons added, reaching a plateau at the C_4x and C_6 complexes.

U–O stretching frequencies

Frequencies of the U–O stretching modes calculated using the PBE functional in the gas phase and in the presence of a DCM continuum solvent are presented in Table 5. In previous

Table 5 Uranyl stretching frequencies from structures calculated using the PBE functional in the gas phase/*DCM*

	ν_{U-Os} (cm^{-1})	ν_{U-Oas} (cm^{-1})
C_0	817.74/*788.41*	897.56/*856.30*
C_2a'	830.41/*800.15*	916.13/*873.18*
C_2b'	834.35/*803.25*	921.88/*878.08*
C_2c'	834.07/*802.73*	921.75/*878.54*
C_4a	836.81/*810.84*	923.95/*887.87*
C_4b	836.02/*813.31*	923.72/*888.99*
C_4c	837.01/*813.26*	923.53/*889.73*
C_6	823.98/*809.39*	909.92/*886.52*

studies, a degree of U–O bond weakening upon equatorial uranyl complexation has been both spectroscopically observed and theoretically calculated,[42,94–97,123,124] with the magnitude of this weakening corresponding to a redshift in the distinctive uranyl stretching modes. Our previous study demonstrated strong correlations between binding energy and the frequency of the uranyl stretching modes in a series of monodentate complexes in which uranyl is coordinated by a first row species.[97]

Fig. 5 shows both the symmetric and asymmetric stretching frequencies of uranyl in C_0, C_2a', C_2b', C_2c', C_4a, C_4b, C_4c and C_6 plotted against the deformation adjusted binding energy. It is immediately clear that such a linear relationship is not present here, with only very weak correlation ($R^2 \leq 0.3$ in all cases). Plotting these frequencies against the uranyl deformation energy however, as seen in Fig. 6, results in weak correlation

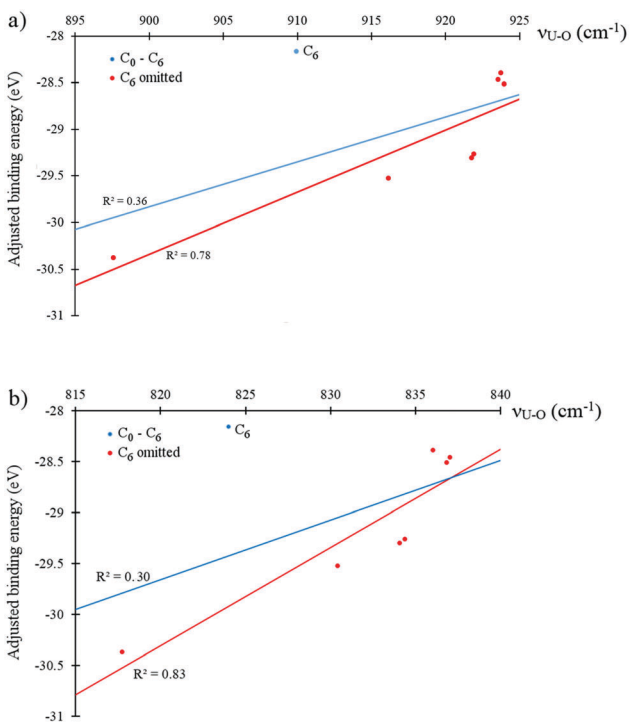

Fig. 5 Linear fitting of the relationship between deformation adjusted binding energies and (a) antisymmetric and (b) symmetric stretching modes of uranyl; fits are given for the entire data sets (blue) and omitting the outlying C_6 results (red). Generated from data obtained using the PBE xc-functional in the gas phase.

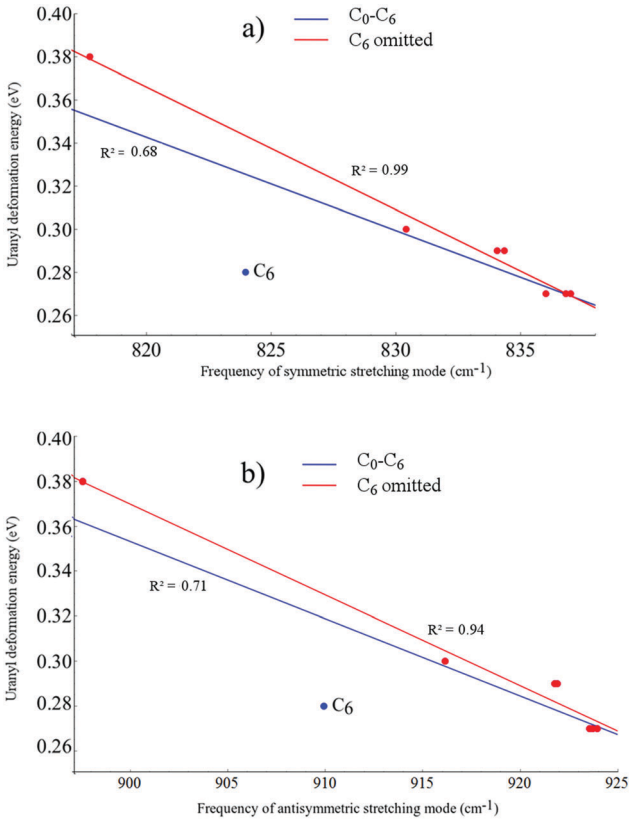

Fig. 6 Linear fitting of the relationship between uranyl deformation energies and the frequencies of (a) the symmetric, and (b) the antisymmetric stretching modes of uranyl. Fit lines are given for the entire data set (blue) and omitting the outlying C_6 result (red). Generated from data obtained using the PBE functional in the gas phase.

(R^2 = 0.68 and 0.71 for the symmetric and asymmetric modes, respectively) with the C_6 complex being an obvious outlier in what is otherwise an apparent linear relationship. When the C_6 complex is omitted from the linear regression analysis, correlation becomes very strong (R^2 = 0.99 and 0.94 for the symmetric and asymmetric modes, respectively). Returning to the relationship between the symmetric/asymmetric stretching frequencies of uranyl and the binding energy/deformation adjusted binding energy, omitting the C_6 complex results in moderate correlation, with R^2 values of between 0.53 and 0.83 and correlation being slightly stronger when considering the adjusted binding energy. Possible reasons for the anomalous behaviour exhibited by the C_6 complex will be further explored in later sections.

For the following density based analysis, a representative set of complexes have been selected. This set comprises C_0, C_2b' (which is the experimentally best characterised C_2x' complex), C_4a (the most stable of the three hypothetical C_4x complexes) and C_6. All are simplified complexes except for C_2b' since, as discussed above, substitution was found to only impact significantly on C_2x geometries. The characterisation will focus on PBE-optimised gas phase complexes, with data from B3LYP-optimised and solvated simulations given in ESI† and discussed where relevant.

Topological analysis of the electron density

Topological properties of the U–N and U–O bonds are now considered. The values of the electron density, ρ, its Laplacian, $\nabla^2\rho$, and the energy density, H, were investigated at the U–N and U–O bond critical point (BCP). Also included in this section is the delocalisation index δ(A,B), defined as the number of electrons delocalised between two atomic basins A and B. Table 6 contains average and total values of topological descriptors at the U–N BCPs. As a rule of thumb, a covalent bond is expected to have an electron density at the bond critical point of $\rho \geq 0.2$ a.u., with a negative Laplacian and an energy density which is negative in sign, with its magnitude commensurate with the degree of covalency.[101,102] It is immediately apparent from the data in Table 6 that, as expected, none of the U–N bonds investigated here exhibit pronounced covalency, rather each U–N bond has a small degree of covalent character which can be quantified by the values of these topological properties at the BCP. Average and total properties are given in Table 6 since it is the effect of the ligand as a whole on the uranyl unit which is of greatest interest, however there is a strong relationship between individual U–N bond lengths in C_0, C_2b', C_4a and C_6 and ρ_{BCP} values, (see Fig. 7) where the shorter the bond, the larger the covalent component of the interaction.

When average values are considered (see Table 7), it can be seen that equatorial covalency decreases and U–N bond length increases in the order $C_0 > C_2b' > C_6 > C_4a$, with C_0 having by far the most U–N covalency and the other three complexes

Table 6 Topological parameters obtained at the bond critical points of the U–N bonds and delocalisation indices between the U–N atomic basins, given as total or average values measured in atomic units (a.u.). Data is from structures calculated using the PBE functional in the gas phase

	C_0	C_2b'	C_4a	C_6
$\sum\rho_{U-N}$	0.350	0.255	0.244	0.248
$\overline{\nabla^2\rho_{U-N}}$	0.149	0.106	0.101	0.103
$\sum H_{U-N}$	−0.042	−0.019	−0.019	−0.018
$\sum\delta$(U,N)	2.143	1.819	1.761	1.766

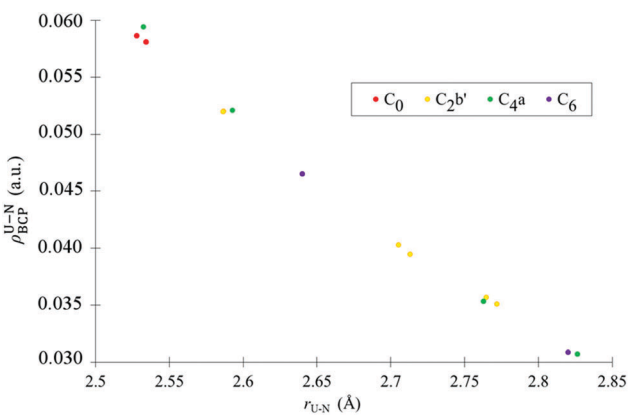

Fig. 7 Values of U–N ρ_{BCP} plotted against individual U–N bond lengths for C_0, C_2b', C_4a and C_6, for complexes optimised using the PBE xc-functional in the gas phase.

Table 7 Average values of ρ_{BCP} and bond lengths for the U–N bonds in C_0, C_2b', C_4a, and C_6, given in Angstrom and a.u., respectively. Data is from structures calculated using the PBE functional in the gas phase

	$\overline{\rho_{U-N}}$	$\overline{r_{U-N}}$
C_0	0.058	2.532
C_2b'	0.042	2.668
C_4a	0.041	2.717
C_6	0.041	2.700

being broadly similar in their U–N character. It is worth emphasising that the U–N bonding character of C_2b', C_4a and C_6 is very similar in comparison to the differences between these complexes and C_0. When the relationship between the frequencies of the uranyl stretching modes and the sum of ρ_{BCP} (see Table 6) for the U–N bonds is investigated, linear regression reveals only weak correlations with R^2 = 0.74 and 0.61 for the antisymmetric and symmetric modes, respectively. The values of the energy density, H, at the BCPs of all U–N bonds, support conclusions drawn from the electron density, ρ, of weak covalent character. H takes negative, albeit very small, values in all complexes, with C_0 having the largest magnitude, indicating the greatest degree of covalent character.

The delocalisation index (see Table 6), summed over all U–N bonds, may be considered a direct measure of electron sharing between the uranyl unit and the ligand. Supporting the assertion based on analysis of ρ_{BCP} that the U–N bonds in C_0 have significantly more covalent character than any of the other complexes, C_0 exhibits the greatest degree of electron delocalisation in its U–N bonds, with C_2b', C_4a and C_6 all exhibiting comparable values, similar to those of the $[UO_2(BTP)_2]^{2+}$ complex we considered previously.[98]

In Table 8, various topological parameters of the U–O bonds are given. We find strong correlation (R^2 = 0.97) between average values of ρ_{BCP} for the U–N bonds and values of ρ_{BCP} for the U–O bonds (see Fig. 8). This can be explained in terms of the effect on the uranyl unit due to the bonding in the equatorial plane, which acts to destabilise it, as we have previously reported,[97,98] resulting in U–O covalency being weakest when equatorial covalency is strongest. Two things are of note when these data are considered. Firstly, C_0 is again set apart from the other complexes, with significantly greater equatorial covalency and a commensurately smaller degree of covalency in the U–O interaction. Secondly, C_6 again appears to differ from the other complexes in that its two U–O bonds have noticeably different values of ρ_{BCP}.

Table 8 Topological parameters obtained at the bond critical points of the U–O bond, and the U–O delocalisation index, measured in atomic units (a.u.). Data is from structures calculated using the PBE xc-functional in the gas phase

	C_0	C_2b'	C_4a	C_6			
	U–O	U–O	U–O	$U–O_1$	$U–O_2$	$O_1–C_m$	$O_2–N$
ρ_{A-B}	0.290	0.299	0.301	0.301	0.299	0.009	—
$\nabla^2\rho_{A-B}$	0.320	0.315	0.314	0.323	0.307	0.037	—
H_{A-B}	−0.253	−0.270	−0.274	−0.272	−0.269	0.002	—
δ(A,B)	1.915	1.971	1.977	1.958	1.961	0.033	0.091

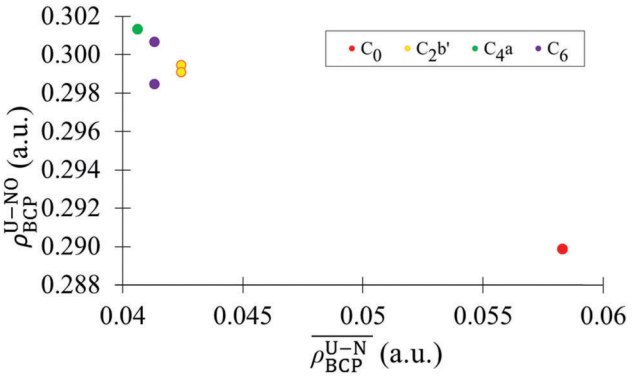

Fig. 8 Average values of ρ_{BCP} for the U–N bonds plotted against values of ρ_{BCP} for the U–O bonds.

This is explained by the fact that C_6 has a characteristic unique amongst the complexes investigated here: QTAIM analysis reveals bond paths between two ligand *meso*-carbons and one of the uranyl oxygens, which is enclosed by the ligand in a manner reminiscent of a Pacman-style complex.[125] Topological properties associated with this interaction are given in Table 8, showing that they are weak non-covalent interactions with ρ_{BCP} an order of magnitude lower than in the U–O bonds. When only the value of ρ_{BCP} for the unenclosed U–O bond in C_6 is used, the frequencies of the uranyl stretching modes and values of ρ_{BCP} for the U–O bonds are found to have an improved linear relationship with R^2 = 0.88 and 0.79 for the antisymmetric and symmetric modes, respectively. When the value of ρ_{BCP} for the enclosed U–O bond of C_6 is used, linear correlations decrease to R^2 = 0.70 and 0.58 for the antisymmetric and symmetric modes, respectively. Thus the uranyl stretching modes in the C_6 complex are significantly perturbed by these additional interactions.

The effect of solvation is to slightly increase topological parameters in all U–N bonds, with a commensurate small decrease in the values of the topological parameters in the U–O bonds (see Tables S6–S9, ESI†). As in our previous work,[97,98] choice of functional appears to have consistent, small, but non-negligible effects on the QTAIM parameters (see Tables S8 and S9, ESI†). For all complexes, use of the hybrid B3LYP xc-functional results in a small but appreciable increase in ρ_{BCP} for the U–O bond, and a small reduction in delocalisation. At the U–N BCPs, optimisation with B3LYP results in a small reduction in all properties measured compared to those obtained using PBE, implying that inclusion of a proportion of exact exchange results in increased electron localisation.[14,48,97,98]

Reduced density gradient

The reduced density gradient (RDG), $s(\mathbf{r}) = |\nabla\rho(\mathbf{r})|/2(3\pi^2)^{1/3}\rho(\mathbf{r})^{4/3}$, has very small values in regions of covalent and predominantly noncovalent interactions,[104,126] tending towards zero at critical points in the electron density. In regions of covalent interactions, $\rho(\mathbf{r})$ is large, and where interactions are largely noncovalent, such as the U–N bonding regions of the complexes under investigation here, $\rho(\mathbf{r})$, as evidenced by our QTAIM analysis, tends to be

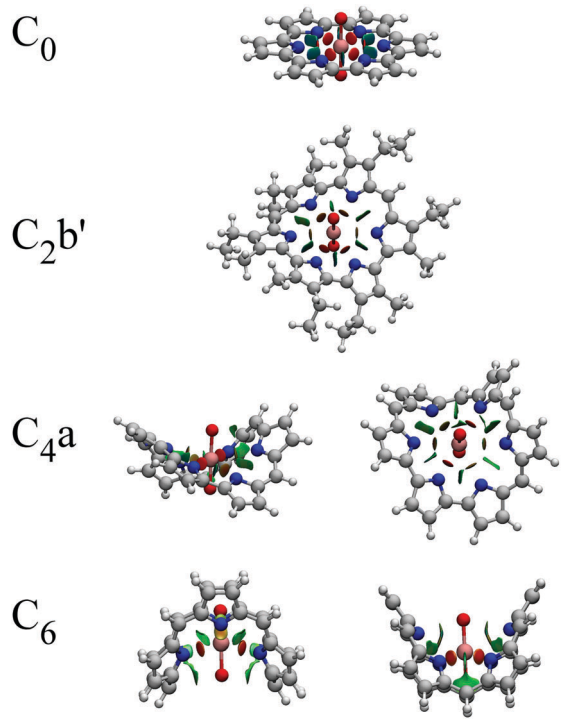

Fig. 9 Isosurfaces of the reduced density gradient, $s(\mathbf{r})$, mapped with values of $\rho(\mathbf{r})\mathrm{sgn}(\lambda_2)$. Red regions indicate attractive interactions with weakly covalent character. Green areas indicate regions of weak interaction which may be attractive or repulsive. Isosurfaces are rendered at $s(\mathbf{r})$ = 0.35 a.u.

small but non-zero. Visualising the $s(\mathbf{r})$ isosurface therefore allows us to qualitatively examine the spatial regions in which these weakly covalent interactions are taking place. These isosurfaces, which are presented in Fig. 9, are colour-mapped with values of $\rho(\mathbf{r})\mathrm{sgn}(\lambda_2)$, where $\mathrm{sgn}(x)$ is the signum function, returning a value of 1 where x is positive, and -1 where x is negative. λ_2 is the second largest eigenvalue of the Hessian of $\rho(\mathbf{r})$ and is typically negative for attractive interactions and positive for repulsive interactions.[127] This allows us to discriminate between attractive and repulsive interactions.

The isosurfaces, plotted at a value of $s(\mathbf{r}) = 0.35$, show regions of weak attraction in each of the U–N bonding regions, with the colouring corresponding to the strength of the interaction, as can be best seen for C_2b'. In all complexes, green regions may be interpreted as either weak steric repulsion or weak attraction between adjacent nitrogen atoms, although a distinction is difficult to make. As the ligands become larger and the complexes more non-planar, we find additional regions of weak interaction, between uranyl oxygen ions and nearby pyrrole units in C_4a, and between the enclosed oxygen ion and interacting *meso*-carbons in C_6. These latter interactions correspond to the bond paths identified between the uranium and *meso*-carbon centres in our QTAIM analysis and, as discussed above, are strong enough to noticeably perturb other molecular properties. Additionally, in C_6, regions of weak interaction between two pyrrolic nitrogen centres and the uranium ion are seen to extend towards the unenclosed oxygen ion, suggesting the possible presence of further ligand-oxygen interactions, although these are not identified by bond paths in our QTAIM analysis.

Scatter plots of $s(\mathbf{r})$ against $\rho(\mathbf{r})\mathrm{sgn}(\lambda_2)$ indicating the presence of largely noncovalent interactions *via* spikes which occur at low densities are given in Fig. S1 (ESI†). In all complexes, $s(\mathbf{r})$ falls to zero at several points, corresponding to critical points in the electron density. $s(\mathbf{r})$ also falls to zero at some small positive values of $\rho(\mathbf{r})\mathrm{sgn}(\lambda_2)$, indicating the presence of weak repulsive interactions.

Integrated properties of the electron density

Using the atomic populations, localisation and delocalisation indices associated with the uranyl unit, the accumulation and depletion of charges which occur upon complexation can be further probed. We define two additional measures,

$$N(\mathrm{UO_2}) = N(\mathrm{U}) + \sum_i N(\mathrm{O}_i) \quad (5)$$

$$\lambda(\mathrm{UO_2}) = \sum_{i=\mathrm{U,O}} \left[\lambda(i) + \frac{1}{2} \sum_{j=\mathrm{U,O} \neq i} \delta(i,j) \right] \quad (6)$$

where $N(\mathrm{UO_2})$ gives the electronic population of the uranyl unit as a whole, and $\lambda(\mathrm{UO_2})$ the number of electrons localised on the uranyl unit. In the case of free UO_2^{2+}, $N(\mathrm{UO_2}) = \lambda(\mathrm{UO_2}) = 106$ but, when complexed, deviations from this value allow insight into the nature of the interaction between the uranyl unit and the ligand, as we have previously reported.[97,98] Table 9 gives the atomic populations, localisation and delocalisation data for the uranyl units in each complex, as well as those of isolated uranyl.

These data allow us to quantify the effect of equatorial complexation by each of the ligands on the uranyl unit. This effect is broadly similar for each of the four complexes, differing only in magnitude. For all complexes $N(\mathrm{UO_2})$ is found to be greater than 106 and, as found in our previous comparison of C_2b, C_2b' and $[UO_2(BTP)_2]^{2+}$,[98] approximately 0.8–0.9 a.u. of electronic charge is donated into the uranyl unit. This additional charge is distributed between the uranium ion and each of the oxygen ions and therefore acts to increase the electrostatic repulsion between the ions.

It might be expected that the localisation index, *i.e.* the amount of electronic charge density localised on an ion, may be used to estimate the strength of an ionic interaction. In all four complexes, greater electron localisation is present on the

Table 9 Integrated properties associated with the uranyl ions of each complex. Data is from structures calculated using the PBE xc-functional in the gas phase

	UO_2^{2+}	C_0	C_2b'	C_4a	C_6
$N(\mathrm{U})$	88.84	89.19	89.17	89.17	89.17
$N(\mathrm{O})$	8.58	8.86	8.84, 8.85	8.84	8.84
$\lambda(\mathrm{U})$	86.52	86.05	86.13	86.15	86.16
$\lambda(\mathrm{O})$	7.35	7.71	7.69	7.66	7.63, 7.61
$\delta(\mathrm{U,O})$	2.32	1.92	1.97	1.98	1.96
$\delta(\mathrm{O_1,O_2})$	0.13	0.10	0.10	0.10	0.10
$N(\mathrm{UO_2})$	106.00	106.90	106.86	106.84	106.85
$\lambda(\mathrm{UO_2})$	106.00	105.40	105.56	105.52	105.41
$N(\mathrm{UO_2})$–$\lambda(\mathrm{UO_2})$	0.00	1.50	1.30	1.32	1.44

oxygen centre compared to free uranyl, alongside a decrease in localisation on the uranium centre, demonstrating that complexation results in increased ionic interaction. Additionally, for all complexes, a reduction in the delocalisation index of the U–O_{yl} bond, δ(U,O), which can be considered an alternative measure of bond covalency, is apparent upon complexation, indicating a reduction in the covalent interaction. This provides evidence that the ionic character of the U–O_{yl} bond is enhanced by equatorial complexation, and the elongation and weakening of the U–O_{yl} bond can thus be understood to originate from the fact that this increased ionic interaction comes at the expense of U–O_{yl} bond covalent interaction. The lengthening and weakening of the U–O bond compared to free uranyl seen in all four complexes investigated here can therefore be attributed to these factors. As might be expected, the effects are most pronounced for C_0, with $N(UO_2)$ being 0.9 a.u. greater and $\lambda(UO_2)$ 0.6 a.u. less than in free uranyl. These values, combined, suggest the greatest amount of electron delocalisation between the uranyl and the ligand, commensurate with the topological data which demonstrates that C_0 has the largest U–N covalent bond character.

This interpretation is in keeping with the qualitative picture given by electron density differences, which show a clear depletion of charge in the U–O_{yl} bonding region along with an accumulation on the O_{yl} centres.

In terms of charge donation onto the uranyl unit, C_2b' and C_4a are similar to one another. C_6 exhibits similar donation to these complexes, but less of this charge is actually localised on the uranyl unit, with C_6 having a $\lambda(UO_2)$ value more comparable to that of C_0, suggesting greater uranyl–ligand delocalisation than can be accounted for by considering the values of δ(U,N). C_6 also has the smallest amount of electronic charge localised on the oxygen centres and the largest amount localised on the uranium centre. This can be explained in terms of the additional interactions between the uranyl oxygen centres and the ligand in this complex. Table 8 shows that, in total, an additional $\sim$0.07 a.u. of charge is delocalised in the interactions between the enclosed oxygen centre with the nearby *meso*-carbons, which partially accounts for the difference between C_6 and C_2b'/C_4a. Based on the RDG isosurface of C_6, further examination of the integrated properties reveals that 0.09 a.u. of charge is delocalised between the unenclosed oxygen ion and each of the two nearby nitrogen atoms, contributing to the lower than expected $\lambda(UO_2)$ value found in C_6 and suggesting that, while ligand–uranyl interactions in planar complexes may be fairly straightforward, in larger, less planar complexes, there are potentially many other interactions which need to be considered in order to explain the charge redistribution in the uranyl unit. This O–N electron sharing also exists in the other complexes considered, but its magnitude is typically only $\sim$50% of that found in C_6.

Solvation, irrespective of which functional is used (see Tables S11 and S13, ESI†), results in slightly higher values of $N(UO_2)$ for all four complexes, while $\lambda(UO_2)$ remains largely unchanged. Reoptimisation with B3LYP (see Tables S12 and S13, ESI†) results in greater localisation compared to the PBE data, as reported in the topological properties. Also apparent are lower values of $N(UO_2)$ (by $\sim$0.1 a.u.) and higher values of $\lambda(UO_2)$ (by $\sim$0.01 a.u.).

Density difference distributions upon complexation

Finally, we use electron density difference distributions to qualitatively examine the changes undergone by the system upon complexation. The density difference distributions in Fig. 10 are generated by subtracting the electron density of uranyl and ligand fragments held at the coordination geometry from the electron density of the complex. This leaves a map of the changes that occur when a complex is formed, with regions of electron density accumulation coloured blue and depletion coloured in green. Regions of depletion on the ligands are evidence of electron donation from the ligand, and the teardrop shaped regions of accumulation in each U–N bonding region may be interpreted as evidence of covalent interactions. It is possible, particularly in C_0 and C_2b', to see that the size of these regions of accumulation varies between the different U–N bonds. The regions of accumulation in C_0 are large and well-focused on the bonds whereas C_2b', exhibits smaller regions for the longest, least covalent bonds and larger regions for the shorter, more covalent interactions. Our previous study[97] has shown that for more ionic uranyl–ligand interactions, these regions of charge accumulation are more diffuse.

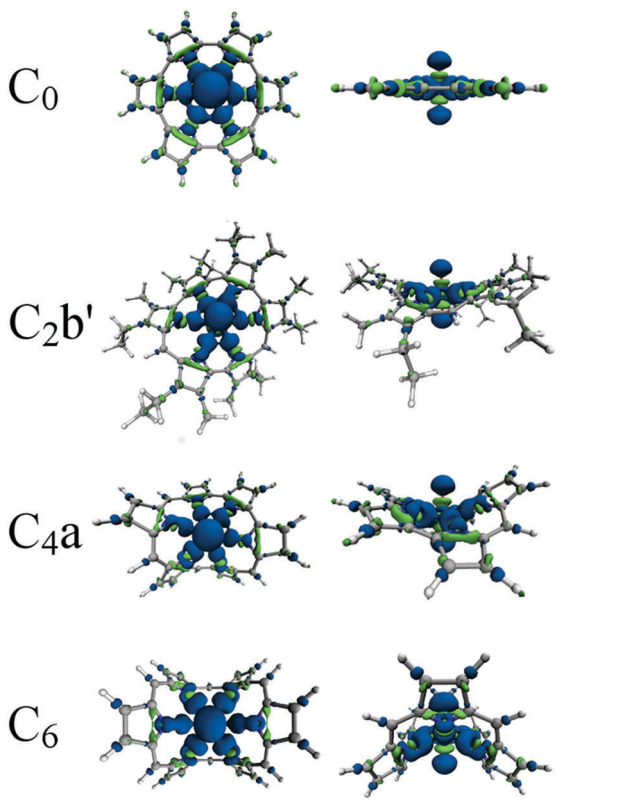

Fig. 10 Electron density differences upon complexation viewed from above, and in the plane of, the ligand. Blue regions indicate charge accumulation and green areas charge depletion. All densities visualised using an isosurface of ρ = 0.005 a.u.

The striking changes undergone by the uranyl unit lend qualitative support to our assertion that there is a significant redistribution of charge in the uranyl unit upon complexation, based on the calculated increased U–O bond lengths, redshifted frequencies of the uranyl stretching modes, uranyl deformation energies and decreased U–O delocalisation, all compared to free UO_2^{2+}. The charge accumulation on the oxygen ions and depletion in the U–O interaction region upon complexation potentially signifies the involvement of density formally associated with the uranium centre with bonding in the U–N region. The depletion in the U–O bond regions is also consistent with a reduction in the covalent character of these bonds, while accumulation on the uranyl oxygen ions and uranium ion suggests that the U–O interaction is, in accord with our other analyses, becoming more ionic upon complexation. In addition to this, charge accumulation around the uranium centre appears to have some f-like character (see Fig. S2, ESI†). The size of the regions of accumulation and depletion on the uranyl unit appear to be related to the interactions in the U–N region, *i.e.* as the amount of electron sharing in the U–N bonds is increased, the effects on the uranyl unit become more pronounced.

Summary and conclusions

We have investigated by means of quantum chemical calculations and a range of density based analyses the U–N and U–O interactions of several uranyl hexaphyrin complexes. It has been determined through a comparison of the geometries of simplified and peripherally substituted complexes that it is of great importance when dealing with systems such as these to ensure that the effects of common simplifications such as the removal of alkyl groups are indeed minimal. This is especially important when dealing with hypothetical complexes. It was found that in most, but not all, cases that removal of the alkyl groups had little geometrical impact.

We initially established a relationship between complex stability and ligand size, as well as a weak relationship between stability and uranyl stretching mode frequencies, when a set of eight complexes were considered. This relationship was significantly weaker than that found by us in a previous study,[97] but could be strengthened by omitting the anomalous data associated with the C_6 complex. Subsequently, justification for considering the C_6 complex as being qualitatively different from the others was found in the density based analysis.

A representative set of four complexes was selected for further analysis. We found a relationship between complex stability and the degree of covalent character as defined by the total value of ρ_{BCP} in the U–N bonds in these complexes. The magnitude of the energy density, H, is also higher for these U–N BCPs than in any other complex. Additionally, there is unambiguous evidence of electron sharing in all U–N bonds, and this is at a maximum for C_0. This complex has short, strong U–N bonds and, commensurately, we see the largest effects on the uranyl unit here: complex C_0 has the most significant reduction in U–O bond covalency when compared to free uranyl, the most significant U–O bond lengthening, and pays the greatest energy penalty in terms deformation of the uranyl unit. Despite this, it is the most stable complex of any we have investigated here, which may, in part, be due to covalent stabilisation from the relatively large amount of electron sharing in the U–N bonds.

Electron delocalisation and covalent character as defined by values of ρ_{BCP} and H in the U–N bonds is reduced for C_2b', C_4a, and C_6, although not drastically so, and these all have bond lengths which are comparable due to the flexibility of the ligands, which contort to better fit the uranyl dication in the cavity. There is an energy penalty for this, however and there is a decrease in stability in the order $C_0 > C_2b' > C_4a > C_6$, a trend which appears to be replicated experimentally: the C_0 and C_2b' complexes are known synthetically, while C_4a and C_6 are not. This energy penalty can be seen using both the molecular binding energies and the ligand deformation energies which decrease and increase, respectively, with increasing ligand size. There is also a limit as to how much this ligand distortion can act to increase the covalent character of the U–N bonds; a notable plateau is found in terms of both stability and U–N covalent bond character for C_4a and C_6. When the frequencies of the uranyl stretching modes are considered, the C_6 data is anomalous, falling somewhere between that of the C_2b' and C_4a complexes. With all complexes but C_6, as in our previous study of complexes involving coordination by 1st row species,[97] there is a degree of equatorial planarity. The interactions between the nitrogen ligands and the uranium ion are more or less perpendicular to the U–O_{yl} axis and, as such, the ligands only interact directly with the U atom and this in turn affects the U–O interaction. However in the C_6 complex we see additional interactions between the uranyl oxygen ion enclosed by the ligand and two of the ligand *meso*-carbons, confirmed by QTAIM analysis and RDG isosurface plots, which also indicate the presence of weak interactions between two pyrrolic nitrogens with the other oxygen ion. These interactions, although weak, act to perturb the frequencies of the uranyl stretching modes as well as the topological and integrated properties of the uranyl unit.

We see dramatic and consistent changes to the uranyl unit upon complexation which are related to the covalent character of interactions in the U–N bonding region as well as the stability of the complex. This is evident in U–O bond lengths, the frequencies of the distinctive uranyl stretching modes (with the exception of C_6, as discussed above), values of QTAIM descriptors and integrated charges, and can be visualised *via* electron density difference distributions. These add qualitative support to our assertions that electron density is redistributed in the uranyl unit upon equatorial complexation, with the magnitude of this redistribution related to the magnitude of the equatorial covalent interaction. Density difference distributions also clearly show charge accumulation in the U–N bonding regions, providing qualitative evidence of electron sharing in these interactions.

Analysis of the reduced density gradient allowed visualisation of the regions of weakly covalent interaction in all complexes, with weak attractive regions corresponding to each U–N bond

found in all cases and, in the C_6 complex, additional interactions between the uranyl oxygen ions and the ligand identified.

Ultimately, we conclude that hexaphyrin ligands coordinate uranyl in a broadly similar way, with the uranium atom coordinated *via* largely ionic interactions with small but measurable amounts of covalent character, to six pyrrolic nitrogen atoms. However, the size of the ligand core has pronounced effects on complex stability. U–N covalent character is found to correlate strongly with bond length, however ligand flexibility and its effects (shortened and thus more covalent U–N bonds, but a loss of stability) mean that no clear relationship can be identified between equatorial covalency and stability in these complexes. However, the interesting changes to the electronic structure of the uranyl unit upon complexation suggest that expanded porphyrins are useful systems for investigating the effects of complexation on the uranyl bond. The complicating factor of additional interactions caused by the proximity of the ligand in C_6 suggest that investigation of complexes which have well-defined planarity may be preferable. If selectivity is indeed driven by covalency, it stands to reason that design of ligands to maximise selective behaviour ought to aim to maximise covalent character. The fact that the most stable complex with the greatest equatorial covalency, C_0, is obtained using the ligand with the smallest core suggests that a fruitful avenue of future research into maximising U–N covalency may be pentapyrrolic complexes of uranyl, of which there are several experimentally realised examples including uranyl pentaphyrin[7] and uranyl superphthalocyanine.[128] Additionally, other actinide complexes of these ligands may be explored in order to assess whether a particular ligand has affinity for a particular actinide.

Acknowledgements

AK thanks the EPSRC for the award of a career acceleration fellowship (grant EP/J002208/2). We would like to acknowledge the use of the EPSRC UK National Service for Computational Chemistry Software (NSCCS) at Imperial College London in carrying out this work, and we also acknowledge the use of the UCL Legion and UCL Grace High Performance Computing Facilities (Legion@UCL and Grace@UCL), and associated support services, in the completion of this work.

References

1 M. Seth, M. Dolg, P. Fulde and P. Schwerdtfeger, *J. Am. Chem. Soc.*, 1995, **117**, 6597–6598.
2 M. Dolg, in *Encyclopedia of Computational Chemistry*, ed. H. F. Schaefer, Wiley, Chichester, 2002.
3 P. Söderlind and A. Gonis, *Phys. Rev. B: Condens. Matter Mater. Phys.*, 2010, **82**, 1–4.
4 G. Schreckenbach and G. A. Shamov, *Acc. Chem. Res.*, 2010, **43**, 19–29.
5 D. Wang, W. F. van Gunsteren and Z. Chai, *Chem. Soc. Rev.*, 2012, **41**, 5836.
6 J. Dognon, *Coord. Chem. Rev.*, 2014, **266–267**, 110–122.
7 J. L. Sessler, A. E. Vivian, D. Seidel, A. K. Burrell, M. Hoehner, T. D. Mody, A. Gebauer, S. J. Weghorn and V. Lynch, *Coord. Chem. Rev.*, 2001, **216–217**, 411–434.
8 P. L. Arnold, J. B. Love and D. Patel, *Coord. Chem. Rev.*, 2009, **253**, 1973–1978.
9 H. H. Dam, D. N. Reinhoudt and W. Verboom, *Chem. Soc. Rev.*, 2007, **36**, 367–377.
10 J. Sessler, P. Melfi and G. Pantos, *Coord. Chem. Rev.*, 2006, **250**, 816–843.
11 V. Alexander, *Chem. Rev.*, 1995, **95**, 273–342.
12 Z. Hnatejko, S. Lis, P. Starynowicz and Z. Stryła, *Polyhedron*, 2011, **30**, 880–885.
13 J.-C. Berthet, M. Nierlich, Y. Miquel, C. Madic and M. Ephritikhine, *Dalton Trans.*, 2005, 369–379.
14 R. Beekmeyer and A. Kerridge, *Inorganics*, 2015, **3**, 482–499.
15 Y. K. Agrawal, P. Shrivastav and S. K. Menon, *Sep. Purif. Technol.*, 2000, **20**, 177–183.
16 J. B. Love, *Chem. Commun.*, 2009, 3154–3165.
17 S. Fortier and T. W. Hayton, *Coord. Chem. Rev.*, 2010, **254**, 197–214.
18 J.-C. Berthet, P. Thuéry, J.-P. Dognon, D. Guillaneux and M. Ephritikhine, *Inorg. Chem.*, 2008, **47**, 6850–6862.
19 J.-C. Berthet, P. Thuéry and M. Ephritikhine, *Chem. Commun.*, 2007, 604–606.
20 K. Pierloot and E. van Besien, *J. Chem. Phys.*, 2005, **123**, 2043091.
21 http://www.nei.org/Knowledge-Center/Nuclear-Statistics/World-Statistics.
22 http://www.nei.org/Knowledge-Center/Nuclear-Statistics/On-Site-Storage-of-Nuclear-Waste.
23 Z. Kolarik, *Solvent Extr. Ion Exch.*, 2003, **21**, 381–397.
24 M. G. B. Drew, M. R. S. J. Foreman, C. Hill, M. J. Hudson and C. Madic, *Inorg. Chem. Commun.*, 2005, **8**, 239–241.
25 F. Lewis, L. Harwood, M. J. Hudson, M. G. B. Drew, J. Desreux, G. Vidick, N. Bouslimani, G. Modolo, A. Wilden, M. Sypula, T.-H. Vu and J.-P. Simonin, *J. Am. Chem. Soc.*, 2011, **133**, 13093–13102.
26 L. Petit, C. Adamo and P. Maldivi, *Inorg. Chem.*, 2006, **45**, 8517–8522.
27 F. W. Lewis, L. M. Harwood, M. J. Hudson, M. G. B. Drew, A. Wilden, M. Sypula, G. Modolo, T. Vu, G. Vidick, N. Bouslimani and J. F. Desreux, *Procedia Chem.*, 2012, **7**, 231–238.
28 C. De Sahb, L. A. Watson, J. Nadas and B. P. Hay, *Inorg. Chem.*, 2013, **52**, 10632–10642.
29 M. Trumm and B. Schimmelpfennig, *Mol. Phys.*, 2016, **114**, 876–883.
30 J. Lan, W. Shi, L. Yuan, Y. Zhao, J. Li and Z. Chai, *Inorg. Chem.*, 2011, **50**, 9230–9237.
31 G. R. Choppin, *J. Alloys Compd.*, 1995, **223**, 174–179.
32 G. R. Choppin, *J. Alloys Compd.*, 1995, **225**, 242–245.
33 P. Söderlind, G. Kotliar, K. Haule, P. M. Oppeneer and D. Guillaumont, *MRS Bull.*, 2010, **35**, 883–888.
34 S. O. Odoh and G. Schreckenbach, *J. Phys. Chem. A*, 2011, **115**, 14110–14119.
35 M. L. Neidig, D. L. Clark and R. L. Martin, *Coord. Chem. Rev.*, 2013, **257**, 394–406.

36 A. Kerridge, *RSC Adv.*, 2014, **4**, 12078–12086.
37 I. Kirker and N. Kaltsoyannis, *Dalton Trans.*, 2011, **40**, 124–131.
38 K. I. M. Ingram, M. J. Tassell, A. J. Gaunt and N. Kaltsoyannis, *Inorg. Chem.*, 2008, **47**, 7824–7833.
39 N. Kaltsoyannis, *Inorg. Chem.*, 2013, **52**, 3407–3413.
40 F. W. Lewis, L. M. Harwood, M. J. Hudson, M. G. B. Drew, M. Sypula, G. Modolo, D. Whittaker, C. A. Sharrad, V. Videva and V. Hubscher-bruder, *Dalton Trans.*, 2012, **41**, 9209–9219.
41 F. W. Lewis, M. J. Hudson and L. M. Harwood, *Synlett*, 2011, 2609–2632.
42 V. Vallet, U. Wahlgren and I. Grenthe, *J. Phys. Chem. A*, 2012, **116**, 12373–12380.
43 L. E. Roy, N. J. Bridges and L. R. Martin, *Dalton Trans.*, 2013, **42**, 2636–2642.
44 J.-H. Lan, W.-Q. Shi, L.-Y. Yuan, J. Li, Y.-L. Zhao and Z.-F. Chai, *Coord. Chem. Rev.*, 2012, **256**, 1406–1417.
45 S. A. Kozimor, P. Yang, E. R. Batista, K. S. Boland, C. J. Burns, D. L. Clark, S. D. Conradson, R. L. Martin, M. P. Wilkerson and L. E. Wolfsberg, *J. Am. Chem. Soc.*, 2009, **131**, 12125–12136.
46 M. J. Tassell and N. Kaltsoyannis, *Dalton Trans.*, 2010, **39**, 6576–6588.
47 A. Kerridge, *Dalton Trans.*, 2013, **42**, 16428–16436.
48 I. Fryer-kanssen, J. Austin and A. Kerridge, *Inorg. Chem.*, 2016, **55**, 10034–10042.
49 M. Mazzanti, R. Wietzke, J. Pécaut, J.-M. Latour, P. Maldivi and M. Remy, *Inorg. Chem.*, 2002, **41**, 2389–2399.
50 D. Guillaumont, *J. Phys. Chem. A*, 2004, **108**, 6893–6900.
51 D. Guillaumont, *THEOCHEM*, 2006, **771**, 105–110.
52 M. A. Denecke, P. J. Panak, F. Burdet, M. Weigl, A. Geist, R. Klenze, M. Mazzanti and K. Gompper, *C. R. Chim.*, 2007, **10**, 872–882.
53 P. J. Melfi, S. K. Kim, J. T. Lee, F. Bolze, D. Seidel, V. M. Lynch, J. M. Veauthier, A. J. Gaunt, M. P. Neu, Z. Ou, K. M. Kadish, S. Fukuzumi, K. Ohkubo and J. L. Sessler, *Inorg. Chem.*, 2007, **46**, 5143–5145.
54 J. L. Sessler, P. J. Melfi, D. Seidel, A. E. V. Gorden, D. K. Ford, P. D. Palmer and C. D. Tait, *Tetrahedron*, 2004, **60**, 11089–11097.
55 J. L. Sessler, A. E. Gorden, D. Seidel, S. Hannah, V. Lynch, P. L. Gordon, R. J. Donohoe, C. Drew Tait and D. Webster Keogh, *Inorg. Chim. Acta*, 2002, **341**, 54–70.
56 S. Hannah, D. Seidel, J. L. Sessler and V. Lynch, *Inorg. Chim. Acta*, 2001, **317**, 211–217.
57 J. L. Sessler and S. J. Weghorn, *Expanded, Contracted & Isomeric Porphyrins*, Elsevier, 1997.
58 J. L. Sessler and D. Seidel, *Angew. Chem., Int. Ed.*, 2003, **42**, 5134–5175.
59 J. L. Sessler and E. Tomat, *Acc. Chem. Res.*, 2007, **40**, 371–379.
60 M. R. Kumar and T. K. Chandrashekar, *J. Inclusion Phenom. Macrocyclic Chem.*, 1999, **35**, 553–582.
61 P. J. Melfi, S. Camiolo, J. T. Lee, M. F. Ali, J. T. McDevitt, V. M. Lynch and J. L. Sessler, *Dalton Trans.*, 2008, 1538–1540.
62 J. L. Sessler, D. Seidel, A. E. Vivian, V. Lynch, B. L. Scott and D. W. Keogh, *Angew. Chem., Int. Ed.*, 2001, **40**, 591–594.
63 S. Shimizu, W. S. Cho, J. L. Sessler, H. Shinokubo and A. Osuka, *Chem. – Eur. J.*, 2008, **14**, 2668–2678.
64 S. Mori, S. Shimizu, J. Y. Shin and A. Osuka, *Inorg. Chem.*, 2007, **46**, 4374–4376.
65 J. L. Sessler, D. Seidel, C. Bucher and V. Lynch, *Chem. Commun.*, 2000, 1473–1474.
66 A. K. Gupta and T. K. Chandrashekar, *Tetrahedron Lett.*, 2001, **42**, 3391–3394.
67 H. Rath, N. Aratani, J. M. Lim, J. S. Lee, D. Kim, H. Shinokubo and A. Osuka, *Chem. Commun.*, 2009, 3762–3764.
68 S.-Y. Kee, J. M. Lim, S.-J. Kim, J. Yoo, J.-S. Park, T. Sarma, V. M. Lynch, P. K. Panda, J. L. Sessler, D. Kim and C.-H. Lee, *Chem. Commun.*, 2011, **47**, 6813–6815.
69 R. Kumar, R. Misra, T. K. Chandrashekar, A. Nag, D. Goswami, E. Suresh and C. H. Suresh, *Eur. J. Org. Chem.*, 2007, 4552–4562.
70 Z. S. Yoon, J. H. Kwon, M.-C. Yoon, M. K. Koh, S. B. Noh, J. L. Sessler, J. T. Lee, D. Seidel, A. Aguilar, S. Shimizu, M. Suzuki, A. Osuka and D. Kim, *J. Am. Chem. Soc.*, 2006, **128**, 14128–14134.
71 R. Misra and T. K. Chandrashekar, *Acc. Chem. Res.*, 2008, **41**, 265–279.
72 S. Shimizu, V. G. Anand, R. Taniguchi, K. Furukawa, T. Kato, T. Yokoyama and A. Osuka, *J. Am. Chem. Soc.*, 2004, **126**, 12280–12281.
73 X. Zhu, S. Fu, W.-K. Wong and W.-Y. Wong, *Tetrahedron Lett.*, 2008, **49**, 1843–1846.
74 J. L. Sessler, P. J. Melfi, E. Tomat and V. M. Lynch, *Dalton Trans.*, 2007, 629–632.
75 J. L. Sessler and S. J. Weghorn, *Expanded, Contracted & Isomeric Porphyrins*, Pergamon, 1997.
76 V. V. Roznyatovskiy, C.-H. Lee and J. L. Sessler, *Chem. Soc. Rev.*, 2013, **42**, 1921–1933.
77 T. K. Chandrashekar and S. Venkatraman, *Acc. Chem. Res.*, 2003, **36**, 676–691.
78 P. J. Chmielewski and L. Latos-Grażyński, *Coord. Chem. Rev.*, 2005, **249**, 2510–2533.
79 M. Stępień, N. Sprutta and L. Latos-Grażyński, *Angew. Chem., Int. Ed.*, 2011, **50**, 4288–4340.
80 J.-Y. Shin, K. S. Kim, M.-C. Yoon, J. M. Lim, Z. S. Yoon, A. Osuka and D. Kim, *Chem. Soc. Rev.*, 2010, **39**, 2751–2767.
81 S. Saito and A. Osuka, *Angew. Chem., Int. Ed.*, 2011, **50**, 4342–4373.
82 Y. Tanaka, J.-Y. Shin and A. Osuka, *Eur. J. Org. Chem.*, 2008, 1341–1349.
83 H. Mori, Y. M. Sung, B. S. Lee, D. Kim and A. Osuka, *Angew. Chem., Int. Ed.*, 2012, **51**, 12459–12463.
84 I. T. Ho, Z. Zhang, M. Ishida, V. M. Lynch, W. Y. Cha, Y. M. Sung, D. Kim and J. L. Sessler, *J. Am. Chem. Soc.*, 2014, **136**, 4281–4286.
85 X. Cao, Q. Li, A. Moritz, Z. Xie, M. Dolg and X. Chen, *Inorg. Chem.*, 2006, **45**, 43–50.
86 P. L. Arnold, D. Patel, A.-F. Pécharman, C. Wilson and J. B. Love, *Dalton Trans.*, 2010, **39**, 3501–3508.

87 A. Yahia, P. L. Arnold, J. B. Love and L. Maron, *Chem. – Eur. J.*, 2010, **16**, 4881–4888.
88 G. M. Jones, P. L. Arnold and J. B. Love, *Chem. – Eur. J.*, 2013, **19**, 10287–10294.
89 Q. J. Pan, G. A. Shamov and G. Schreckenbach, *Chem. – Eur. J.*, 2010, **16**, 2282–2290.
90 J. Silver, *Inorg. Chim. Acta*, 1988, **44**, 281–288.
91 J. H. Lan, C. Z. Wang, Q. Y. Wu, S. A. Wang, Y. X. Feng, Y. L. Zhao, Z. F. Chai and W. Q. Shi, *J. Phys. Chem. A*, 2015, **119**(1), 9178–9188.
92 G. A. Shamov and G. Schreckenbach, *J. Phys. Chem. A*, 2006, **110**, 9486–9499.
93 M. Yang, W. Ding and D. Wang, *New J. Chem.*, 2017, **41**, 63–74.
94 F. Quilès and A. Burneau, *Vib. Spectrosc.*, 2000, **23**, 231–241.
95 C. Nguyen-Trung, D. A. Palmer, G. M. Begun, C. Peiffert and R. E. Mesmer, *J. Solution Chem.*, 2000, **29**, 101–129.
96 F. Quilès, C. Nguyen-Trung, C. Carteret and B. Humbert, *Inorg. Chem.*, 2011, **50**, 2811–2823.
97 P. Di Pietro and A. Kerridge, *Inorg. Chem.*, 2016, **55**, 573–583.
98 P. Di Pietro and A. Kerridge, *Phys. Chem. Chem. Phys.*, 2016, **18**, 16830–16839.
99 A. E. Clark, J. L. Sonnenberg, P. J. Hay and R. L. Martin, *J. Chem. Phys.*, 2004, **121**, 2563–2570.
100 P. Miro, J. Ling, J. Qiu, P. C. Burns, L. Gagliardi and C. J. Cramer, *Inorg. Chem.*, 2012, **51**, 8784–8790.
101 R. F. W. Bader, *Atoms in Molecules: A Quantum Theory*, Oxford University Press, Oxford, 1990.
102 C. F. Matta and R. J. Boyd, *An Introduction to the Quantum Theory of Atoms in Molecules*, 2007.
103 R. F. W. Bader, *J. Phys. Chem. A*, 2009, **113**, 10391–10396.
104 E. R. Johnson, S. Keinan, P. Mori-Sánchez, J. Contreras-García, A. J. Cohen and W. Yang, *J. Am. Chem. Soc.*, 2010, **132**, 6498–6506.
105 R. Ahlrichs, M. Bär, M. Häser, H. Horn and C. Kölmel, *Chem. Phys. Lett.*, 1989, **162**, 165–169.
106 F. Weigend and R. Ahlrichs, *Phys. Chem. Chem. Phys.*, 2005, **7**, 3297–3305.
107 W. Küchle, M. Dolg, H. Stoll and H. Preuss, *J. Chem. Phys.*, 1994, **100**, 7535.
108 J. Perdew, K. Burke and M. Ernzerhof, *Phys. Rev. Lett.*, 1996, **77**, 3865–3868.
109 A. D. Becke, *J. Chem. Phys.*, 1993, **98**, 5648.
110 P. Stephens, F. Devlin, C. Chabalowski and M. Frisch, *J. Phys. Chem.*, 1994, **98**, 11623–11627.
111 N. Ismail, J.-L. Heully, T. Saue, J.-P. Daudey and C. J. Marsden, *Chem. Phys. Lett.*, 1999, **300**, 296–302.
112 G. Schreckenbach, P. J. Hay and R. L. Martin, *J. Comput. Chem.*, 1999, **20**, 70–90.
113 A. Klamt and G. Schüürmann, *Perkin Trans. 2*, 1993, 799–805.
114 G. A. Shamov and G. Schreckenbach, *Inorg. Chem.*, 2008, **47**, 805–811.
115 D. A. Pantazis and F. Neese, *J. Chem. Theory Comput.*, 2011, **7**, 677–684.
116 N. M. Kroll and M. Douglas, *Ann. Phys.*, 1974, **83**, 89–155.
117 B. A. Hess, *Phys. Rev. A: At., Mol., Opt. Phys.*, 1986, **33**, 3742–3748.
118 T. Lu and F. Chen, *J. Comput. Chem.*, 2012, **33**, 580–592.
119 T. A. Keith, *AIMAll (Version 14.11.23), TK Gristmill Software*, Overl. Park KS, USA, 2014.
120 W. Humphrey, A. Dalke and K. Schulten, *J. Mol. Graphics*, 1996, **14**, 33–38.
121 P. L. Arnold, D. Patel, A.-F. Pécharman, C. Wilson and J. B. Love, *Dalton Trans.*, 2010, **39**, 3501–3508.
122 Q.-J. Pan, S. O. Odoh, G. Schreckenbach, P. L. Arnold and J. B. Love, *Dalton Trans.*, 2012, **41**, 8878–8885.
123 S. Tsushima, *Dalton Trans.*, 2011, **40**, 6732–6737.
124 D. D. Schnaars and R. E. Wilson, *Inorg. Chem.*, 2013, **52**, 14138–14147.
125 J. B. Love, *Chem. Commun.*, 2009, 3154–3165.
126 A. Zupan, K. Burke, M. Ernzerhof and J. P. Perdew, *J. Chem. Phys.*, 1997, **106**, 10184.
127 R. F. W. Bader and H. Essén, *J. Chem. Phys.*, 1984, **80**, 1943.
128 V. W. Day, T. J. Marks and W. A. Wachter, *J. Am. Chem. Soc.*, 1975, **505**, 4519–4527.